

X-ray spectral complexity in narrow-line Seyfert 1 galaxies

S. Vaughan¹, J. Reeves¹, R. Warwick¹, R. Edelson^{1,2}

¹*X-Ray Astronomy Group; Department of Physics and Astronomy; Leicester University; Leicester LE1 7RH; U.K.*

²*Department of Physics and Astronomy; University of California, Los Angeles; Los Angeles, CA 90095-1562; U.S.A.*

Submitted 30 March 1999; Revised version 11 May 1999; Accepted 20 May

ABSTRACT

We present a systematic analysis of the X-ray spectral properties of a sample of 22 “narrow-line” Seyfert 1 galaxies for which data are available from the ASCA public archive. Many of these sources, which were selected on the basis of their relatively narrow $H\beta$ line width ($\text{FWHM} \leq 2000$ km/s), show significant spectral complexity in the X-ray band. Their measured hard power-law continua have photon indices spanning the range 1.6 – 2.5 with a mean of 2.1, which is only slightly steeper than the norm for “broad-line” Seyfert 1s. All but four of the sources exhibit a soft excess, which can be modelled as blackbody emission ($T_{bb} \approx 100 - 300$ eV) superposed on the underlying power-law. This soft component is often so strong that, even in the relatively hard bandpass of ASCA, it contains a significant fraction, if not the bulk, of the X-ray luminosity, apparently ruling out models in which the soft excess is produced entirely through reprocessing of the hard continuum.

Most notably, 6 of the 22 objects show evidence for a broad absorption feature centred in the energy range 1.1–1.4 keV, which could be the signature of resonance absorption in highly ionized material. A further 3 sources exhibit “warm absorption” edges in the 0.7–0.9 keV bandpass. Remarkably, all 9 “absorbed” sources have $H\beta$ line widths below 1000 km/s, which is less than the median value for the sample taken as a whole. This tendency for very narrow line widths to correlate with the presence of ionized absorption features in the soft X-ray spectra of NLS1s, if confirmed in larger samples, may provide a further clue in the puzzle of active galactic nuclei.

Key words: galaxies: active – galaxies: Seyfert – X-rays: galaxies – accretion, accretion disks

1 INTRODUCTION

Significant hard X-ray luminosity is now regarded as one of the defining characteristics of Seyfert 1 galaxies. X-ray spectral and variability observations establish that the emission is produced in the innermost regions of the Seyfert nucleus and provide a means of investigating both the nuclear geometry and the processes accompanying accretion onto a supermassive black-hole (e.g. Mushotzky, Done & Pounds 1993).

The hard X-ray spectra of normal Seyfert 1s can, to first order, be described in terms of a power-law continuum with a photon index of typically $\Gamma = 1.9$ (Nandra & Pounds 1994). In many sources additional spectral features are observed, such as a spectral turn-up above 10 keV and strong iron $K\alpha$ fluorescence in the 6 - 7 keV band, which can be attributed to Compton reflection of the continuum by optically thick matter, possibly in the form of an accretion disk (e.g. George & Fabian 1991; Matt, Perola & Piro 1991). The presence of

a soft X-ray excess may in turn represent the high energy tail of the thermal emission generated in the inner regions of the disc (e.g. Czerny & Elvis 1987). Recent interest has also focussed on the detection of “warm absorption” features in the soft X-ray spectra of Seyfert 1 galaxies which are an imprint of highly photoionized material lying in the line of sight to the nuclear source (Reynolds 1997; George et al. 1998).

Narrow-line Seyfert 1s (NLS1s) represent a subclass of objects occupying one extreme of the measured range of optical line widths, *i.e.* $H\beta$ $\text{FWHM} \leq 2000$ km/s (Osterbrock & Pogge 1985). Observations with *ROSAT* have shown that NLS1s frequently have stronger soft excesses and increased variability in the 0.1–2 keV band than more normal, “broad-line” Seyfert 1s (hereafter BLS1s; Boller, Brandt & Fink 1996). A possible explanation of the extreme properties of NLS1s is that these are active galactic nuclei (AGN) containing black holes of relatively modest mass which, nevertheless, are accreting at a high rate (Pounds, Done & Os-

arXiv:astro-ph/9905323v1 25 May 1999

borne 1995). In this model, the lower mass black hole gives rise to smaller Keplerian velocities of the broad-line region clouds while the high accretion rate yields comparable luminosity to that of larger mass black holes and leads to increased disc emission and an enhanced soft excess (Ross, Fabian & Mineshige 1992). In some NLS1s there is tentative evidence for reflection from a highly ionized disc (e.g. Comastri et al. 1998), which fits naturally with the high accretion rate model, as the disc surface is expected to be highly ionized (Matt, Fabian & Ross 1993). Recent studies suggest that NLS1s, in addition to their extreme soft X-ray spectra, also exhibit steeper intrinsic hard X-ray continua than their broad-line counterparts (e.g. Brandt, Mathur & Elvis 1997), an effect which could arise, for example, if the strong soft excess effectively cools the accretion disk corona in which the underlying power-law is formed (Pounds, Done & Osborne 1995; Maraschi & Haardt 1997)

Our objective in this paper is to investigate the X-ray spectral properties of a sample of NLS1s. Specifically we are interested in whether there are any further X-ray spectral characteristics of NLS1s, over and above those noted earlier, which might be described as distinctive of this class of object. In practical terms we have carried out a systematic analysis of 24 observations of 22 NLS1s taken from the *ASCA* public data archive. The remainder of this paper is organised as follows. In the next section we define the source sample and detail the observations and data reduction techniques. In Section 3 we go on to describe the results of our X-ray spectral analysis and in Section 4 present a discussion of these results. Finally we summarise our conclusions in Section 5.

2 OBSERVATIONS AND DATA REDUCTION

We have selected 22 objects, identified in the literature as Seyfert 1 galaxies or quasars with $H\beta$ FWHM ≤ 2000 km/s, for which *ASCA* data were available at the time of the analysis (late 1998). The sample, given in Table 1, is not complete in any sense except that it consists of all suitable spectra of NLS1s in the *ASCA* public archive. The redshift distribution of the sample is shown in Fig. 1. The NLS1 galaxy Mkn 957 was also observed by *ASCA* but these data have not been analysed due to the very short exposure time of the observation (~ 3 ks). In addition data on Kaz 163 have been excluded; Kaz 163 is in the same GIS field as Mkn 507 but its image falls at the extreme edge of the SIS detector, making the data unsuitable for detailed spectral analysis.

ASCA carries four instruments which are operated simultaneously namely two solid-state imaging spectrometers (SIS-0 and SIS-1; Burke et al. 1991) and two gas imaging spectrometers (GIS-2 and GIS-3; Kohmura et al. 1993). In the current analysis, standard data screening criteria were applied to all the data. Table 1 lists the resulting exposure times (specifically for SIS-0, although data from all four *ASCA* instruments are utilised here). Since we are concerned only with the spectral properties of the sources, time-averaged spectra have been extracted from each observation. Counts were accumulated, where possible, in circular apertures of 3–4 arcmin radius centred on the source. The background was estimated using source free regions from the same observation and, in the case of the GIS observations,

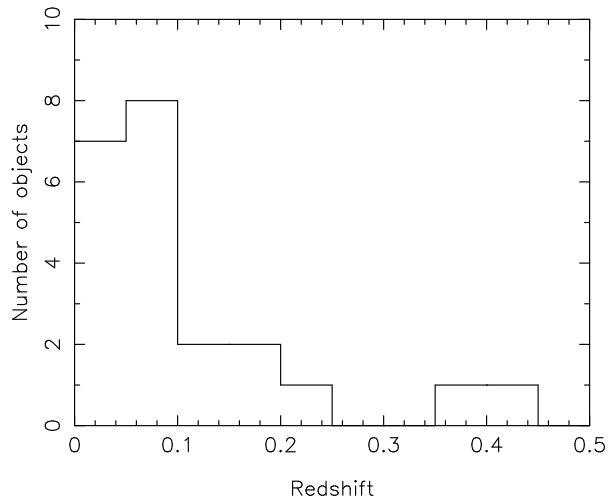


Figure 1. The redshift distribution of the NLS1 sample.

at a similar off-axis angle to the source. After background subtraction the pulse height spectra were binned to give at least 20 counts per spectral channel. In the subsequent analysis the SIS data were restricted to the 0.6–10 keV energy range and GIS data to the 0.8–10 keV band so as to reduce the possible impact of calibration uncertainties.

As a check of the possible impact of spectral variability on the time-averaged source spectra, we extracted the 2–10 keV and 0.5–2.0 keV light curves of each source (SIS-0 and SIS-1 co-added) and binned these on the satellite orbital timescale (5760 s). We then used a χ^2 test to check the constancy of the spectral hardness (defined as ratio of the 2–10 keV count rate to the 0.5–2.0 keV count rate) during the observation. Five out of 22 sources gave unacceptable values of χ^2 at the 95% level (NAB 10205+024, RX J0439–45, NGC 4051, Mkn 478, Ark 564) indicative of underlying spectral variability. However, with the exception of NGC 4051 there was little evidence that these variations corresponded to any clear spectral trends or to a systematic effect (e.g. a spectral hardness versus flux correlation). We conclude that the implicit assumption of the analysis which follows, namely that the observation-averaged spectra provide a good representation of the source properties, is a reasonable one.

3 X-RAY SPECTRAL ANALYSIS

Spectral fitting of the binned source spectra was carried out using the XSPEC v10.0 software package. In general, data from all four detectors have been fitted simultaneously, but with the relative normalisations of the spectra free to vary between the four instruments. The quoted errors on the derived best-fitting model parameters correspond to a 90% confidence level for one interesting parameter (*i.e.* a $\Delta\chi^2 = 2.7$ criterion) unless otherwise stated. Values of $H_0 = 50$ km/s/Mpc and $q_0 = 0.5$ are assumed throughout this section and fit parameters (specifically the emission and absorption line energies) are quoted for the rest frame of the source.

Table 1. The *ASCA* NLS1 sample. The columns contain the following information: (1) The source name; (2) The sequence number of the observation; (3) & (4) The observation pointing position; (5) The exposure time for SIS-0 (ks); (6) The line-of-sight Galactic hydrogen column density from Dickey & Lockman (1990) (in units of 10^{20} cm $^{-2}$); (7) The source redshift; (8) The H β line width (km/s); (9) References to the information in columns (7) & (8).

Name	<i>ASCA</i>	RA	Dec	SIS-0	N_H	z	H β FWHM	Ref.
(1)	Sequence (2)	(J2000) (3)	(J2000) (4)	Exp. (5)	(6)	(7)	(8)	(9)
Mkn 335	71010000	00 06 04	20 11 12	18	3.99	0.026	1640	1
I Zw 1	73042000	00 53 41	12 46 40	27	4.99	0.061	1240	2
Ton S180	74081000	00 57 28	-22 17 50	44	1.55	0.062	1000	2
PHL 1092	75042000	01 40 01	06 24 32	68	4.07	0.396	1300	2
RX J0148-27	75048000	01 48 30	-27 53 19	34	1.42	0.121	1050	3
NAB 0205+024	74071000	02 07 44	02 38 02	41	3.51	0.155	1050	4
RX J0439-45	75050000	04 40 14	-45 39 46	43	2.02	0.224	1010	3
PKS 0558-504	74096000	06 00 04	-50 22 06	33	4.39	0.137	1500	2
1H 0707-495	73043000	07 08 26	-49 37 47	34	5.80	0.040	1000	2
RE J1034+39 (1)	72020000	10 35 04	39 40 28	28	1.02	0.042	1500	2
RE J1034+39 (2)	72020010	10 34 14	39 36 05	11	1.02	0.042	1500	2
Mkn 42	75056000	11 53 12	46 11 26	36	1.99	0.024	670	2
NGC 4051 (1)	70001000	12 03 06	44 32 33	25	1.32	0.002	990	2
NGC 4051 (2)	72001000	12 02 43	44 29 50	69	1.32	0.002	990	2
PG 1211+143	70025000	12 14 13	14 03 32	13	2.74	0.080	1860	1
PG 1244+026	74070000	12 46 17	02 19 24	37	1.75	0.048	830	1
IRAS 13224-3809	72011000	13 24 52	-38 25 57	82	4.79	0.067	650	2
PG 1404+226	72021000	14 06 06	22 22 50	34	2.14	0.098	880	1
Mkn 478	73067000	14 41 43	35 24 57	29	1.03	0.079	1450	2
PG 1543+489	75059000	15 46 00	48 48 06	39	1.59	0.400	1560	1
IRAS 17020+454	73047000	17 03 09	45 36 52	35	2.22	0.060	490	2
Mkn 507	74033000	17 49 00	68 37 26	32	4.38	0.056	960	2
IRAS 20181-224	73075000	20 20 53	-22 40 10	51	5.96	0.185	580	2
Ark 564	74052000	22 42 34	29 38 21	47	6.40	0.024	750	2

REFERENCES: (1) Wang et al. (1996). (2) Brandt (1996). (3) Grupe (1996). (4) Zheng & O'Brien (1990).

3.1 Initial spectral fits

Broadly, our strategy has been to apply relatively simple spectral models, so as to characterize the properties of the whole sample of sources. Thus initially a model comprising just a power-law continuum with absorption due to the line-of-sight Galactic N_H (see Table 1) was employed as a way of illustrating the variety of X-ray spectra exhibited by NLS1 galaxies. Fig. 2 shows the residuals from these fits for all 24 observations, which in most instances have unacceptable minimum χ^2 values. cursory inspection of Fig. 2 shows that soft excesses are often present below ~ 2 keV and that broad absorption and/or emission complexes are also evident in a number of the sources. In general, an iron K α emission-line is difficult to pick out (by eye), although NGC 4051 provides the exception. In one source, Mkn 507 the largest residual occurs in the lowest spectral channel suggesting the possibility of cold absorption over and above the Galactic column density. In this case we obtain an improved fit ($\Delta\chi^2 = 12$) when the N_H is allowed to be a free parameter, the specific value derived being $N_H = 3.2 \pm 1.5 \times 10^{21}$ cm $^{-2}$ (see Iwasawa, Brandt & Fabian 1998). In the rest of this paper we assume that Mkn 507 is the only NLS1 in the sample with excess cold absorption.

3.2 The 2–10 keV spectral form

In order to characterize better the hard X-ray spectrum of each NLS1, we next excluded all the spectral data below

2 keV, where evidently soft excesses and warm absorbers add to the spectral complexity. The 2–10 keV spectra were again fitted with a simple power law plus Galactic absorption model but with the addition of a narrow Gaussian emission line ($\sigma = 0.01$ keV) to represent iron K α emission in the 6.4–7.0 keV bandpass. Table 2 summarizes the results. Acceptable fits were found for most sources, with only three instances of (reduced) $\chi^2_{\nu} \geq 1.1$. We note that the derived photon indices have a mean value of 2.1 with a standard deviation of 0.3.

For nine objects the inclusion of the iron-line component is merited in terms of the resulting improvement in χ^2 (*i.e.* $\Delta\chi^2 > 6.2$ implying better than 95% confidence in the F-test for two additional parameters). Also two further sources show at least a marginal improvement in χ^2 (see Table 2). There is some evidence for lines originating from fairly highly ionized iron species (*i.e.* $> \text{FeXX}$ and above) in I Zw 1, Ton S180, PKS 0558-504, PG 1244+026 and Ark 564. The measured line equivalent widths range from 100–600 eV, albeit with large uncertainties. Similarly the constraints on the equivalent width of a (neutral) iron line in those sources lacking a significant line detection are generally rather weak. In general the signal/noise ratio was too poor to meaningfully constrain the intrinsic line widths. However, the second observation of NGC 4051 provides the exception in this case there is evidence for a broadened iron K α feature. The best fit parameters for the line are $E = 6.29 \pm 0.09$ keV, intrinsic width $\sigma = 0.36_{-0.15}^{+0.23}$ keV and $\text{EW} = 240_{-80}^{+90}$ eV. The improvement in the fit upon adding this broad feature is

$\Delta\chi^2 = 76.8$. An attempt has been made to fit the line with the relativistic “diskline” profile of Fabian et al. (1989); we find a mildly ionized line ($E = 6.6^{+0.1}_{-0.2}$ keV), with a near to face-on inclination ($i < 17^\circ$) gives the best fit to the data (assuming values for R_{in} , R_{out} and emissivity index of $10GM/c^2$, $100GM/c^2$ and -2 , respectively). Note that Guainazzi et al. (1996) discuss the the spectral fitting of this *ASCA* observation of NGC 4051 in some detail.

3.3 The soft X-ray spectra

Extrapolation of the best-fit 2–10 keV spectrum (as defined in Table 2) down to 0.6 keV in most cases results in a poor fit of the soft X-ray spectrum, with the most common residual feature being an excess of soft flux. In the spectral fitting we have attempted to match this soft excess with an additional continuum component. Specifically we use a single blackbody component, although a second power law often provides an equally good fit. (In the latter case the second power-law is typically steeper than the first by $\Delta\Gamma \simeq 0.5$ with a break energy in the range 1–2 keV). Table 3 summarises the results of fitting a power law plus blackbody model (note that from here on the iron line parameters are frozen at the values obtained in the earlier 2–10 keV fits). In all but four objects (I Zw 1, PG 1543+489, Mkn 507 and IRAS 20181–224) a soft excess component provides a significant improvement in the fit, demonstrating that soft excesses are a very common feature in NLS1s. The underlying power-law photon indices given in Table 3 have a mean of 2.12 and a standard deviation of 0.26. The fact the mean is very similar to that obtained earlier for 2–10 keV fits demonstrates that the latter fits are relatively immune to the presence of the soft excess.

Nine objects show signs of additional spectral complexity below 2 keV even after the inclusion of the blackbody component in the fit (Table 3). Unfortunately modelling of the *ASCA* spectra in terms of additional soft X-ray features is not particularly straight-forward. Radiation damage to the CCDs and other factors have meant that there is increasing uncertainty in the calibration of the detectors below 1 keV and, in particular, it has been noted that the two SIS instruments often give divergent spectra at the lowest energies (although these calibration uncertainties only dominate over uncertainties in the background subtraction for relatively bright sources). Also since most NLS1 galaxies appear to exhibit a soft X-ray excess it is difficult to distinguish subtleties in the form of the soft continuum from the effects of putative broad emission and/or absorption features.

Recent studies of the X-ray spectra of NLS1s (e.g. Leighly et al. 1997b; Fiore et al. 1998) have established that in addition to classical “warm-absorption” features, NLS1s often show anomalous absorption features in the 1–2 keV band. Both types of absorption are spectrally complex and will merit more detailed analysis using the predictions of appropriate photoionization codes, once high sensitivity X-ray data with good spectral resolution become available from missions such as AXAF, XMM and ASTRO-E (e.g. Nicastro et al. 1999). However, for our present purpose we have taken a very simplistic approach and have attempted to improve the χ^2 in the spectral fits for nine sources noted above

Table 4. X-ray spectral fitting of a Gaussian absorption line. The columns give the following information: (1) The source name; (2) The best fit line energy (keV); (3) The line equivalent width (eV); (4) The intrinsic line width (keV); (5) The improvement in the fit when the absorption feature is included (compared to Table 3).

Name (1)	Energy (2)	EW (3)	σ (4)	$\Delta\chi^2$ (5)
Ton S180	$1.22^{+0.07}_{-0.04}$	-95 ± 16	0.31 ± 0.04	20
1H 0707-495	1.08 ± 0.03	-112^{+25}_{-38}	0.14 ± 0.07	32
NGC 4051	0.83 ± 0.03	-33^{+4}_{-21}	$0.15^{+0.15}_{-0.02}$	43
PG 1244+026	$1.31^{+0.07}_{-0.03}$	-108 ± 50	0.24 ± 0.08	24
IRAS 13224-38	1.10 ± 0.07	-275^{+120}_{-160}	$0.24^{+0.06}_{-0.03}$	87
PG 1404+226	1.16 ± 0.05	-100 ± 30	0.09 ± 0.02	31
IRAS 17020+45	$0.70^{+0.05}_{-0.02}$	-129^{+25}_{-35}	0.12 ± 0.05	64
IRAS 20181-22	0.90 ± 0.03	-42^{+61}_{-24}	< 1.6	8
Ark 564	1.38 ± 0.03	-55^{+24}_{-10}	$0.19^{+0.11}_{-0.03}$	132

by including just a *single* absorption feature (in the form of a broad Gaussian absorption line) in the spectral model.

Table 4 lists for each of the nine sources the line energy, the equivalent width and the intrinsic line width obtained when such an absorption feature is added to the power-law plus blackbody continuum model. The line energies are not consistent with a single value but a bifurcation is suggested, namely absorption either in the 0.7–0.9 keV range or in the 1.1–1.4 keV range. Absorption features in the former range are usually interpreted as due to OVII and OVIII edges indicative of the presence of ionized material along the line of sight. The possible origin of the “anomalous” absorption features observed at ~ 1.2 keV have recently been discussed by Leighly et al. (1997b) and Fiore et al. (1998).

As noted above the fitting of a Gaussian absorption feature is necessarily an over simplification of the true picture. In order to investigate the individual sources in somewhat more detail we have refitted the spectra of the nine objects listed in Table 4 including a variety of additional absorption and emission components. For example, we tested for either one or two absorption edges and also for either a single Gaussian emission line or a MEKAL-type optically thin thermal spectrum (Kaastra & Mewe 1993). The outcome was that in five of the objects an absorption component gave a significantly better fit than an emission component. (Of course the modelling of the underlying soft excess changes substantially between these two cases so as to maintain the match to the observed spectrum in the 0.6–2 keV bandpass). Unfortunately the situation is more ambiguous in the remaining cases since absorption and emission models can be constructed which give fairly comparable fits to the *ASCA* data. Further comments on the spectral fitting of the individual nine sources are given in the Appendix.

4 DISCUSSION

4.1 The X-ray continua of NLS1s

Using spectral measurements compiled from the published literature Brandt et al. (1997) identify a correlation between the hard power-law spectral index and the width of the optical $H\beta$ line in a sample of Seyfert 1 galaxies, in the sense that NLS1s tend to have somewhat steeper hard X-ray spectra

Table 2. The results of the 2–10 keV spectral fitting. The columns give the following information: (1) The source name; (2) The power-law photon index; (3) The 2–10 keV flux (10^{-13} erg cm $^{-2}$ s $^{-1}$); (4) The 2–10 keV luminosity (10^{43} erg s $^{-1}$); (5) The iron line energy (keV); (6) The iron-line equivalent width (eV); (7) The improvement in the fit when the iron line is included; (8) The *reduced* χ^2 and number of degrees of freedom for the best fitting model.

(1)	Γ_{2-10} (2)	Flux $_{2-10}$ (3)	L $_{2-10}$ (4)	E $_{Fe}$ (5)	EW $_{Fe}$ (6)	$\Delta\chi^2_{Fe}$ (7)	χ^2_{ν}/dof (8)
Mkn 335	1.89 ± 0.05	109.0	3.2	6.41 ± 0.08	193 ± 78	16.3	1.00/458
I Zw 1	2.27 ± 0.10	34	5.9	6.73 $^{+0.15}_{-0.30}$	450 $^{+250}_{-225}$	11.0	1.04/262
Ton S180	2.39 ± 0.05	45.3	8.3	6.65 ± 0.10	180 ± 90	10.9	1.05/591
PHL 1092	1.67 ± 0.30	3.6	32.0	–	< 490	–	1.18/132
RX J0148–27	1.99 ± 0.17	8.5	5.7	6.5 ± 0.2	670 ± 300	8	0.86/87
NAB 0205+024	2.10 ± 0.09	26.8	30	–	< 122	–	0.85/327
RX J0439–45	2.25 ± 0.16	10.3	22.0	–	< 220	–	1.09/149
PKS 0558–504	2.25 ± 0.04	121	110	6.65 $^{+0.35}_{-0.20}$	65 ± 40	6.5	0.98/820
1H 0707–495	2.40 ± 0.20	9.6	0.7	–	< 375	–	1.04/114
RE J1034+39 (1)	2.46 ± 0.23	10.2	0.7	–	< 490	–	1.08/98
RE J1034+39 (2)	2.73 ± 0.40	8.6	0.7	–	< 1560	–	0.97/32
Mkn 42	2.01 ± 0.17	10.5	0.3	–	< 380	–	0.93/122
NGC 4051 (1)	1.91 ± 0.03	291	0.045	6.43 ± 0.04	145 ± 40	35.6	1.00/905
NGC 4051 (2)	1.84 ± 0.02	234	0.040	6.37 ± 0.03	127 ± 25	66.5	1.06/1449
PG 1211+143	2.03 ± 0.10	34	9.7	6.38 $^{+0.12}_{-0.20}$	260 ± 130	10.7	0.94/342
PG 1244+026	2.35 ± 0.10	26.8	2.8	7.0 ± 0.1	460 ± 210	11	0.99/255
IRAS 13224–3809	1.55 ± 0.22	5.16	1.0	–	< 290	–	1.12/182
PG 1404+226	1.6 ± 0.4	6.4	2.4	–	< 1220	–	0.84/57
Mkn 478	1.92 ± 0.10	25	7.0	6.38 $^{+0.18}_{-0.10}$	200 ± 135	5.7	1.02/216
PG 1543+489	2.46 ± 0.32	4.0	37.2	–	< 350	–	0.87/76
IRAS 17020+454	2.20 ± 0.06	78.4	12.6	6.5 ± 0.5	95 ± 70	5	0.87/577
Mkn 507	1.61 ± 0.30	6.7	9.3	–	< 715	–	1.02/50
IRAS 20181–224	2.33 ± 0.12	10.4	17.5	–	< 120	–	1.14/185
Ark 564	2.50 ± 0.03	205.7	5.2	7.0 ± 0.3	123 ± 50	15	0.99/1171

Table 3. The full 0.6–10 keV spectral fits. The columns give the following information: (1) The source name; (2) The power-law photon index; (3) The blackbody temperature (eV); (4) The 0.6–10 keV flux (10^{-13} erg cm $^{-2}$ s $^{-1}$); (5) The derived unabsorbed luminosity (10^{43} erg s $^{-1}$); (6) The ratio of the 0.6–10 keV luminosities of the blackbody and power-law components; (7) The improvement in the fit when the blackbody component is added; (8) The *reduced* χ^2 and number of degrees of freedom for the best fit model.

Name (1)	Γ (2)	kT (3)	Flux $_{0.6-10}$ (4)	L $_{0.6-10}$ (5)	L $_{bb}/L_{pl}$ (6)	$\Delta\chi^2$ (7)	χ^2_{ν}/dof (8)
Mkn 335	1.96 ± 0.04	160 ± 14	191	5.7	0.12	125	1.01/757
I Zw 1	2.30 ± 0.03	150 ^f	72	14.0	< 0.01	–	0.94/594
Ton S180	2.36 ± 0.05	190 ± 5	137	24.7	0.29	226	1.10/988
PHL 1092	1.67 ± 0.11	162 ± 15	7.0	73	0.80	112	1.12/268
RX J0148–27	2.15 ± 0.15	129 $^{+32}_{-124}$	18.3	12.7	0.15	12	0.91/230
NAB 0205+024	2.10 ± 0.08	218 ± 19	53	63	0.16	36	0.98/697
RX J0439–45	2.28 ± 0.10	137 ± 11	27.4	81	0.58	152	1.02/379
PKS 0558–504	2.26 ± 0.03	230 ± 15	257	247	0.08	34	1.03/1217
1H 0707–495	2.33 ± 0.10	107 ± 4	39.6	3.7	1.21	429	1.29/338
RE J1034+39 (1)	2.35 ± 0.13	131 ± 9	32.8	2.7	0.64	104	0.95/298
RE J1034+39 (2)	2.45 ± 0.20	142 ± 20	33.6	2.8	0.49	23	0.78/125
Mkn 42	1.89 $^{+0.17}_{-0.09}$	227 ± 40	20.6	0.53	0.15	8	0.99/271
NGC 4051 (1)	1.97 ± 0.02	86 ± 5	561	0.10	0.22	824	1.04/1205
NGC 4051 (2)	1.94 ± 0.01	106 ± 5	402	0.07	0.11	1160	1.13/1846
PG 1211+143	2.07 ± 0.06	110 ± 12	72	23.0	0.17	57	0.95/713
PG 1244+026	2.31 ± 0.08	210 ± 10	75	8.1	0.26	64	1.17/535
IRAS 13224–3809	1.60 ± 0.13	119 ± 4	18	4.7	2.1	537	1.28/426
PG 1404+226	1.87 ± 0.20	115 ± 7	12.9	9.1	1.9	177	1.20/167
Mkn 478	1.96 ± 0.05	89 ± 12	50	14.5	0.23	101	1.03/495
PG 1543+489	2.48 ± 0.20	436 ± 436	10.7	105	0.04	1	0.91/206
IRAS 17020+454	2.21 ± 0.05	260 ± 36	148	29	0.05	9	1.06/972
Mkn 507	1.74 ± 0.24	150 ^f	8.6	1.5	< 0.08	–	0.96/97
IRAS 20181–224	2.33 ± 0.11	258 $^{+62}_{-79}$	19.3	47.4	0.08	3	1.15/389
Ark 564	2.44 ± 0.03	195 ± 4	568	16.7	0.21	558	1.27/1567

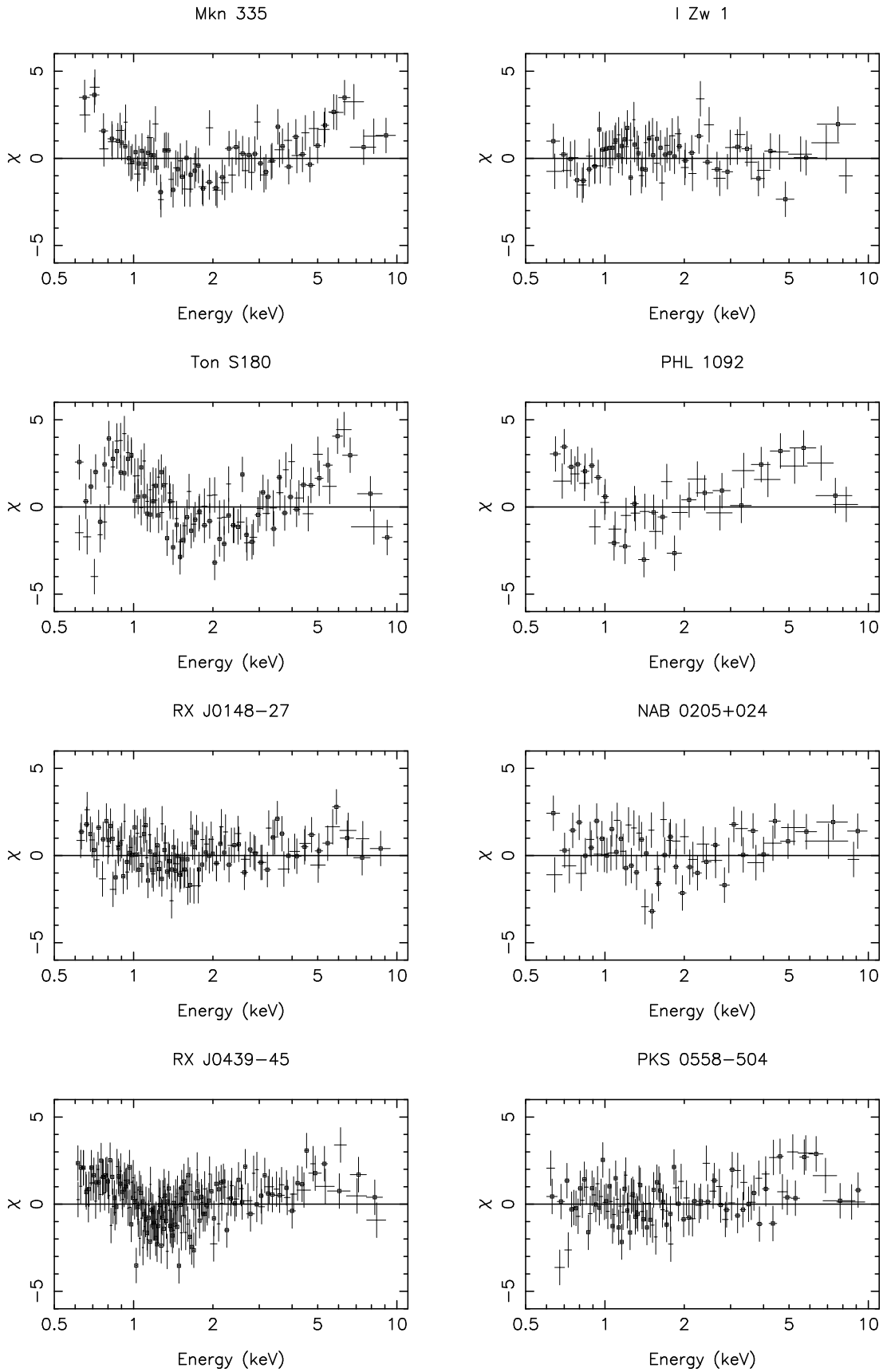
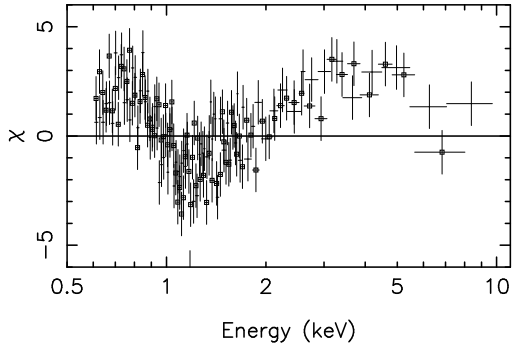
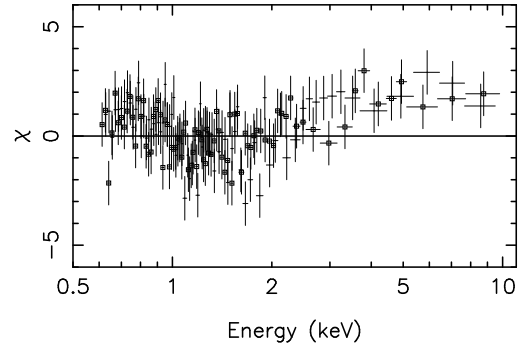


Figure 2. The residuals from spectral fits to the 0.6–10.0 keV *ASCA* spectra using a power-law plus Galactic absorption model. The residuals are in terms of sigmas, with error bars of size one. For clarity only the SIS data are shown, and the SIS-0 data are marked by squares.

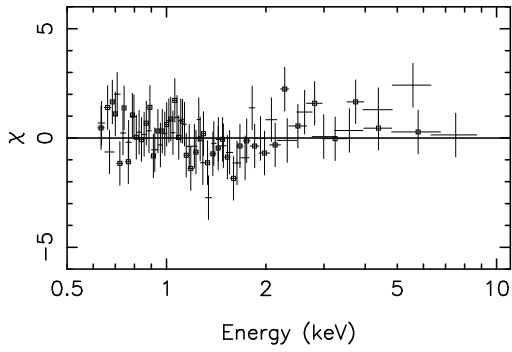
1H 0707-495



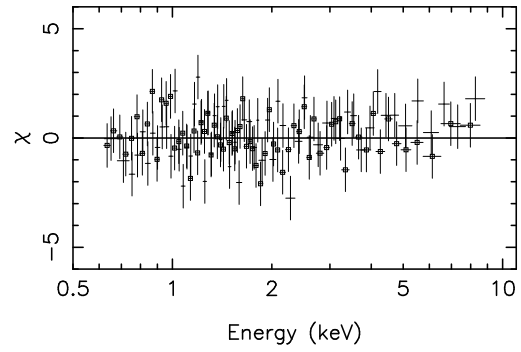
RE J1034+39 (1)



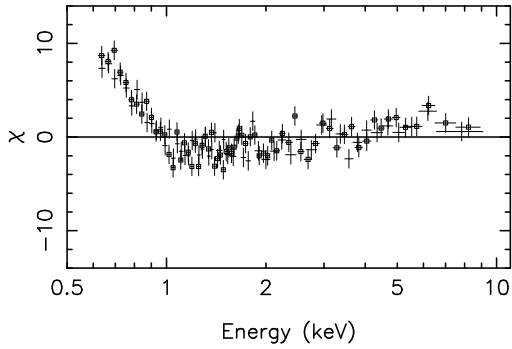
RE J1034+39 (2)



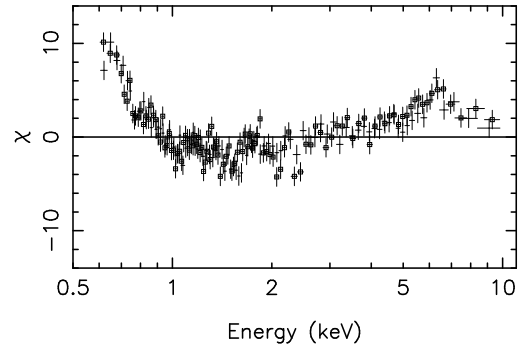
Mkn 42



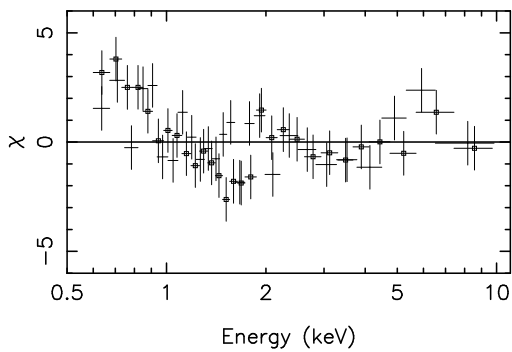
NGC 4051 (1)



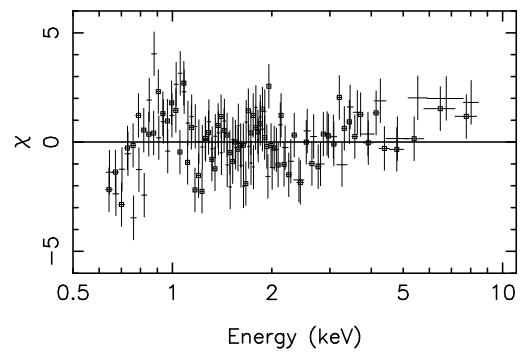
NGC 4051 (2)



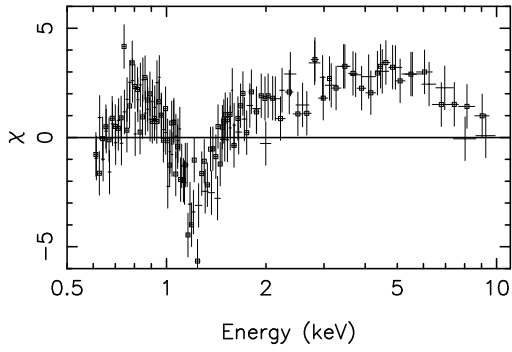
PG 1211+143



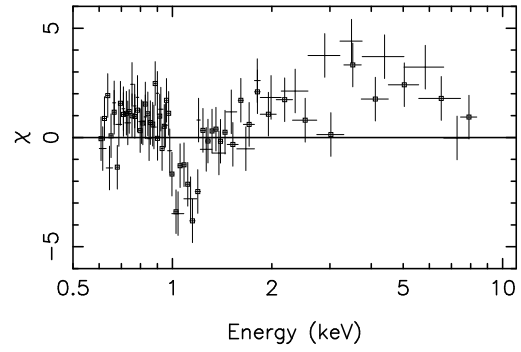
PG 1244+026



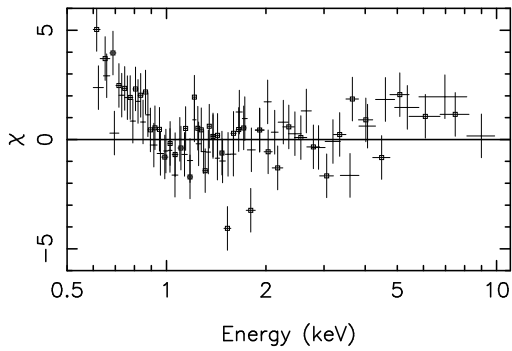
IRAS 13224–3890



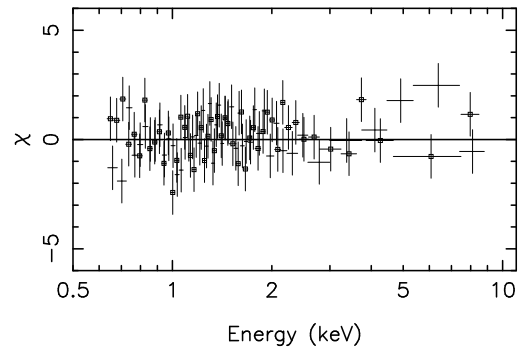
PG 1404+226



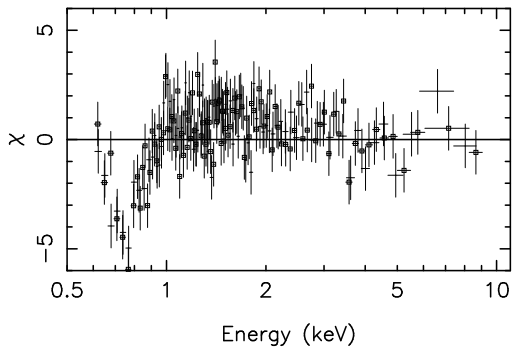
Mkn 478



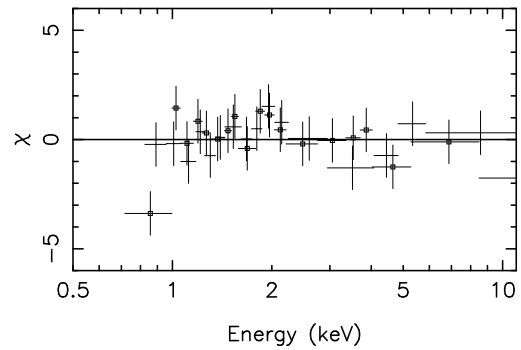
PG 1543+489



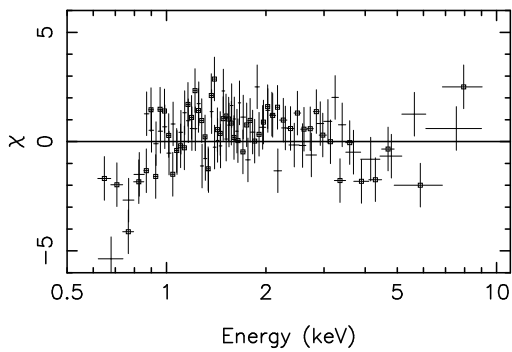
IRAS 17020+454



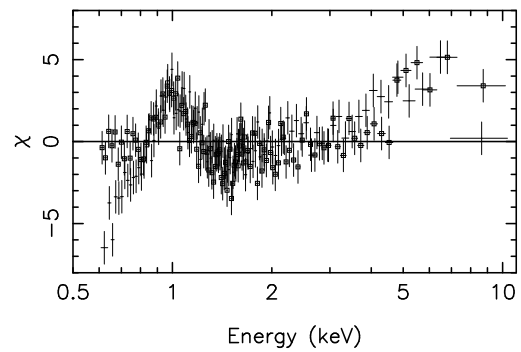
Mkn 507



IRAS 20181–224



Ark 564



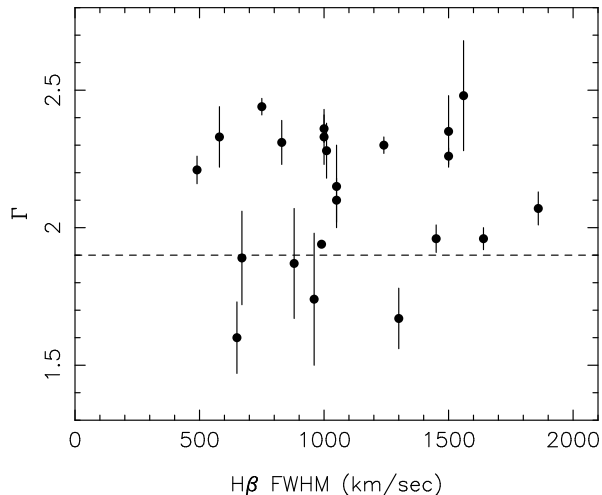


Figure 3. The photon index of the hard continuum plotted against the $H\beta$ line width for the NLS1 sources in the *ASCA* sample. The dotted line represents the mean spectral index of the BLS1 sample of Nandra et al. (1997).

than normal broad-line objects. Fig. 3 shows a plot of power-law photon index (from Table 3) against the $H\beta$ FWHM line width for our source sample. Clearly within the restricted range of line width which defines the NLS1 subclass (*i.e.* $H\beta$ FWHM ≤ 2000 km s $^{-1}$) there is no hint of a correlation. As noted earlier the mean photon index of our sample of NLS1s is $\Gamma = 2.12$, with a standard deviation of $\sigma = 0.26$. Nandra et al. (1997) tabulate the 3–10 keV spectral slopes for 15 BLS1s based on *ASCA* measurements. These give an average slope of $\Gamma = 1.9$ with a standard deviation of $\sigma = 0.17$. Thus a modest trend in Γ over a broad range of $H\beta$ line width is suggested, consistent with the Brandt et al. (1997) result. However, we caution that the spectral steepening is a fairly subtle effect and the above comparison may not be entirely free of selection bias. For example, one could argue that the comparison is of a hard X-ray selected sample with one largely selected at soft X-rays (but see the discussion in Brandt et al. 1997). In counterbalance is the fact that Nandra et al. (1997) include a reflection component in their analysis, which can have the effect of increasing the derived power-law spectral indices by up to $\Delta\Gamma \simeq 0.1$. Thus it is possible that magnitude of the spectral steepening trend noted above is understated.

In the present analysis we have fitted the soft excess in terms of a single temperature blackbody component, which should be a reasonable assumption, given the restricted *ASCA* bandpass, if the emission resembles that expected from an accretion disc (e.g. Ross et al. 1992). Indeed, the addition of a blackbody component significantly improves the fit (at the $> 99\%$ confidence level in the F-test) in 18 out of 22 objects. This is a much higher rate of incidence of soft excesses than appears to be the case for BLS1 samples (e.g. Turner & Pounds 1989; Reynolds 1997). The soft excess generally dominates over the hard power law at energies $\lesssim 1.5$ keV, and presumably peaks in the extreme ultraviolet. Even in the limited *ASCA* bandpass the luminosity of the soft excess is comparable to that of the hard power law and in three objects (1H 0707–495, IRAS 13224–3809 and

PG 1404+226), the blackbody component contains more luminosity than the power law in the 0.6–10 keV range, *i.e.*, $L_{bb}/L_{pl} \geq 1$ (see Table 3). For these three sources, extrapolation of the continuum spectrum down to 0.15 keV and up to 100 keV still leaves this ratio above unity. The implication is that, at least in these NLS1s, the soft excess cannot solely be due to reprocessing of the hard X-ray continuum. (Note for these three objects the soft excess is still dominant even after the inclusion of additional spectral features, see the Appendix.)

Two objects with strong soft excesses, namely PHL 1092 and IRAS 13224–3809, appear to have particularly hard underlying X-ray continua ($\Gamma = 1.6 - 1.7$, see Table 3). This could be used as an argument against models where the soft photons Compton scatter against the hot electrons in an accretion disk corona to produce the underlying X-ray hard spectrum. However, an alternative view might be that the relatively flat 2–10 keV spectra are the result of strong reflection in these objects. Sensitive broadband X-ray spectral measurements (extending well above the Compton peak) would help distinguish between these two descriptions.

4.2 Iron $K\alpha$ emission

Emission lines at 6–7 keV are detected at a modestly significance level in 9 objects with a marginal indication of such lines in 2 others. However, as noted earlier the line properties (energy, equivalent width, intrinsic width) are in general only poorly constrained by the *ASCA* spectra. A point of interest, for follow-up when more sensitive X-ray spectra are available, is the incidence of emission lines from highly ionized gas (corresponding to FeXX and above) in NLS1s, for which the current data provide only a fleeting glimpse.

4.3 Soft X-ray spectral features

The residuals to the best fitting continuum models show unusual features below 2 keV in nine objects. In three sources (NGC 4051, IRAS 17020+454 and IRAS 20181–224) we are probably detecting OVII and OVIII edges at 0.74 and 0.87 keV respectively, indicative of the presence of “warm” absorbing gas in our line of sight to the nuclear continuum source. Of the other six objects, three (1H 0707–495, IRAS 13224–3809 and PG 1404+226) are most likely affected by absorption, whereas for the others (Ton S180, PG 1244+026 and Ark 564) the interpretation is more ambiguous (see the Appendix). However, for the purpose of the present discussion we pursue the assumption adopted earlier, namely that all six sources exhibit anomalous absorption in the range 1.1–1.4 keV with the equivalent width of the absorption feature being typically ~ 100 eV and its intrinsic width (when modelled as a pure Gaussian) ranging from 0.1–0.3 keV (see Table 4 and Fig. 4).

Leighly et al. (1997b) have recently reported the detection of the same anomalous absorption features in three sources and discussed possible physical origins of the effect. Specifically these authors note that in order to identify the absorption with either an OVII and/or an OVIII edge, as predicted in the warm absorber scenario, then very significant (*i.e.* relativistic) outflow velocities would be required in

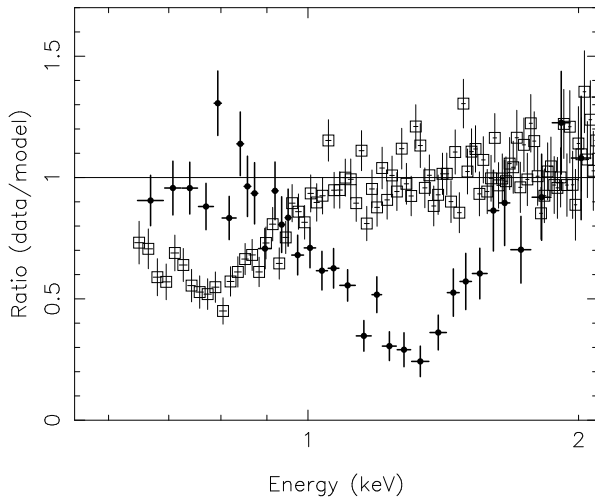


Figure 4. The ratio of the *ASCA* data to the best-fit continuum model for two sources, IRAS 13224–3809 (filled circles) and IRAS 17020+454 (open squares). The former source exhibits an anomalous absorption feature near 1.2 keV and the latter probably a warm (OVII) edge near 0.74 keV. Both spectra have been shifted into the source rest frame and for clarity only SIS-0 data are shown.

order to achieve the necessary blueshifting of the edge energies. An alternative model has been suggested by Nicastro, Fiore & Matt (1999) who invoke resonant absorption lines in a warm absorber to explain the absorption evident in the spectrum of IRAS 13224-3809, in which case there is no requirement for relativistic outflow. The basis of their model is that a steep soft X-ray spectrum can produce a different ionization structure in the warm absorber, with carbon and oxygen fully stripped. Absorption is then produced by a complex of absorption lines around 1–2 keV, made up of mainly iron L resonance lines (see figure 4 of Nicastro et al. 1999). The total equivalent widths of these lines can be ~ 100 eV, consistent with our results, although of course our assumption of a Gaussian absorption profile is in this case an extremely crude approximation to the true underlying spectral form.

On the basis of the above arguments, it is at least plausible that both the 0.7–0.9 keV and the 1.1–1.4 keV absorption arises due to the presence of highly ionized gas along the line of sight to the nuclear X-ray source. Interestingly the two different types of absorbers (described earlier as “warm” and “anomalous”) occupy very different regions of parameter space in Fig. 5, which shows the ratio of the luminosities of the soft excess to the hard power law components (L_{bb}/L_{pl}) versus the $H\beta$ line width. The sources with anomalous absorption clearly tend to have relatively high L_{bb}/L_{pl} values whereas the three sources exhibiting “normal” warm absorption are found at the low end this range. This is circumstantial evidence in support of the Nicastro et al. (1999) model, in that they require a strong contribution from the soft excess in order to produce the necessary conditions for the dominance of resonance over pure photoelectric absorption. This point is given further weight if we also consider BLS1s in that over 50% of such sources show signs of absorption in the range 0.7–0.9 keV, most likely due to oxygen edges, but relatively few possess conspicuous

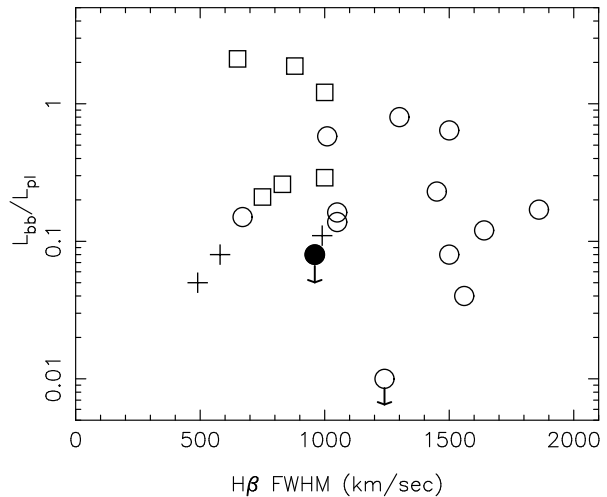


Figure 5. The relative luminosity of the soft excess compared to the hard power law (as given in Table 3) versus the $H\beta$ line width. Objects with no evidence for absorption are marked by circles and those with normal warm absorbers by crosses. The sources exhibiting anomalous 1.1–1.4 keV absorption are marked by squares and Mkn 507 (with possible cold absorption) is marked with a filled circle. The arrows indicate upper limits on the strength of the soft excess.

soft excesses, at least in the *ASCA* bandpass (e.g., Reynolds 1997; George et al. 1998).

A further interesting result illustrated by Fig. 6 is the fact that all but one of the NLS1s with $H\beta$ FWHM ≤ 1000 km/s show evidence for some sort of absorption, either by ionized material or (as in one case) by neutral gas. Conversely none of the NLS1s with $H\beta$ FWHM > 1000 km/s exhibit signs of line-of-sight absorption. One possibility is that this represents a very sharply tuned geometry dependence. For example, if the absorbing material originates in an outflow from the disc, it would only be seen in low inclination systems (for a discussion of the “pole-on” model for NLS1s, see Boller et al. 1996 and references therein). It is unclear, however, why such an incredibly tight upper-limit should apply to the $H\beta$ line width in such circumstances. Clearly further study of this effect using both a larger sample of NLS1s and a more sophisticated modelling of the putative absorption features is merited.

5 CONCLUSIONS

Our analysis of the *ASCA* X-ray spectral data for a sample of 22 NLS1s has revealed a number of important characteristics of this subclass of X-ray source. Absorption from *neutral* gas intrinsic to the host galaxy appears to be a very rare occurrence in NLS1. On the contrary most NLS1s exhibit a soft excess superposed on the hard power-law continuum. Modelled as a blackbody component, this soft excess often contains a significant fraction of the X-ray luminosity in these sources, even in the restricted *ASCA* bandpass. In the most extreme cases this presents an argument against an origin for the soft excess in the reprocessing of the hard continuum. The underlying power-law spectra span a wide range

of slopes ($\Gamma = 1.6 - 2.5$) with a mean spectral index of 2.1, which is slightly steeper than the norm for BLS1s. Iron $K\alpha$ emission lines are detected at a modestly significance level in roughly half of the objects observed, but unfortunately the line properties such as centroid energy, equivalent width and intrinsic width are in general rather poorly constrained by the *ASCA* data.

The X-ray spectra of NLS1s below 2 keV often exhibit additional features, which in the current paper we have interpreted as largely due to absorption by ionized material in the line of sight. Three of the NLS1s show evidence for an absorption in the 0.7–0.9 keV range, probably arising from OVII and OVIII edges, “warm absorber” features which are commonly observed in BLS1s. However, six NLS1s also show spectral features which we take to be absorption in the 1.1–1.4 keV bandpass arising from resonance absorption in highly ionized material. A potentially very important result is that all objects showing signs of absorption by highly ionized gas lie in the lower half of the $H\beta$ line width distribution (*i.e.* the absorbed sources have $H\beta$ FWHM ≤ 1000 km s $^{-1}$). The combination of high effective area, good spectral resolution and extended bandwidth afforded by future missions such as XMM, AXAF and Astro-E, should allow unambiguous identification of the spectral features which appear to characterise NLS1 galaxies and also confirm whether ionized absorption systems are preferentially observed in NLS1s with extremely narrow $H\beta$ line widths.

ACKNOWLEDGMENTS

We thank Paul O’Brien and Ken Pounds for useful discussions, and the referee, Neil Brandt, for his careful reading of the paper and comments. This research made use of data obtained from the Leicester Database and Archive Service (LEDAS) at the Department of Physics and Astronomy, Leicester University, from the High Energy Astrophysics Science Archive Research Center (HEASARC), at the NASA Goddard Space Flight Center and also from the NASA/IPAC Extragalactic Database (NED) at JPL. SV acknowledges support from PPARC in the form of a research studentship.

REFERENCES

- Brandt, W. N., Fabian, A. C., Nandra, K., Reynolds, C. S., Brinkmann, W. 1994, MNRAS, 271, 958
 Brandt, W. N. 1996, Ph.D. Thesis
 Brandt, W. N., Mathur, S., Elvis, M. 1997, MNRAS, 285, L25
 Burke, B. E., Mountain, R. W., Harrison, D. C., Bautz, M. W., Doty, J. P., Ricker, G. R., Daniels, P. J. 1991, IEEE Trans, ED-38, 1069
 Boller, Th., Brandt, W. N., Fink H. H. 1996, A&A 305, 53
 Comastri, A., et al. 1998, A&A, 333, 31
 Czerny, B., Elvis, M. 1987, ApJ, 321, 305
 Dickey J. M., Lockman F. J. 1990, ARA&A 28, 215
 Fabian, A. C. et al. 1989, MNRAS, 238, 729
 Fiore, F., et al. 1998, MNRAS, 298, 103
 George, I. M., Fabian, A. 1991, MNRAS, 249, 352
 George, I. M., Turner, T. J., Netzer, H., Nandra, K., Mushotzky, R. F., Yaqoob, T. 1998, ApJS, 114, 73
 Grupe, D. 1996, Ph.D. Thesis

- Guinazzi, M., Mihara, T., Otani, C., Matsuoka, M. 1996, PASJ, 48, 781
 Iwasawa, K., Brandt, W.N., Fabian, A.C. 1998, MNRAS, 293, 251
 Leighly, K. M., Kay, L. E., Wills, B. J., Wills, D., Grupe, D. 1997a, ApJ, 489, L137
 Leighly, K., Mushotzky, R., Nandra, K., Forster., K. 1997b, ApJ, 489, L25
 Kaastra, J. S., Mewe, R. 1993, A&AS, 97, 443
 Kohmura, Y., et al. 1993, Proc SPIE, 2006, 78
 Komossa, S., Bade, N. 1998, A&A, 331, L49
 Maraschi, L., Haardt, F. 1997, In IAU Colloquium 163, ASP Conference Series, ed. D. T. Wickramasinghe, G. V. Bicknell and L. Ferrario, 121,101
 Matt, G., Fabian, A., Ross, R. 1993, MNRAS, 262, 179
 Matt, G., Perola, G.C., Piro, L. 1991, A&A, 247, 25
 Mushotzky, R.F., Done, C., Pounds, K.A. 1993, ARA&A, 31, 717
 Nandra, K., Pounds, K. A. 1994, MNRAS, 268, 405
 Nandra, K., George., I. M., Mushotzky, R. F., Turner, T. J., Yaqoob, T. 1997, ApJ, 477, 602
 Nicastro, F., Fiore, F., Matt, G. 1999, ApJ, in press
 Osterbrock, D. E., Pogge, R. 1985, ApJ 297, 166
 Pounds, K., Done, C., Osborne, J. 1995, MNRAS, 277, L5
 Reynolds, C. S. 1997, MNRAS, 286, 513
 Ross, R., Fabian, A., Mineshige, S. 1992, MNRAS, 258, 189
 Turner., T., Pounds, K. 1989, MNRAS, 240, 833
 Wang, T., Brinkmann, W., Bergeron, J. 1996, A&A, 309, 81
 Zheng, W., O’Brien, P. T. 1990, ApJ, 353, 433

6 APPENDIX

Some comments on the spectral fitting of individual objects

Ton S180

It is difficult to differentiate between absorption and emission at ~ 1.2 keV in Ton S180. A single absorption edge at a rest energy of $E = 1.09 \pm 0.03$ keV with an optical depth $\tau = 0.17 \pm 0.03$, yields $\chi^2/\nu = 1072/986$. A second edge in the spectrum (at $E = 1.42 \pm 0.06$ keV with $\tau = 0.13 \pm 0.03$) improves the fit further ($\chi^2/\nu = 1059/985$). There is some evidence for an additional edge at ~ 0.73 keV ($\chi^2/\nu = 1048/983$) presumably corresponding to OVII. However SIS-1 seems to underestimate the flux compared to SIS-0 below 0.8 keV, so any features in the spectrum below 0.8 keV need to be considered with caution.

A significant improvement over the soft excess fit is given when a broad Gaussian emission component is added to the model near 1 keV. The best-fit parameters are line $EW = 20 \pm 8$ eV, energy $E = 0.94 \pm 0.03$ keV and intrinsic width $\sigma = 0.062 \pm 0.025$ keV, for which $\chi^2/\nu = 1055/985$. A MEKAL model also gives an acceptable fit to the data, yielding a plasma temperature of $kT = 0.89 \pm 0.11$ keV ($\chi^2/\nu = 1050/986$).

1H 0707-495

An absorption feature definitely gives the best fit in 1H 0707–495. A broad absorption line improves the fit significantly ($\chi^2/\nu = 404/335$), as per Table 4. An equally good

χ^2 can be obtained, but for 1 additional free parameter, using two edges instead of a single Gaussian; the first edge is at $E=1.09 \pm 0.03$ keV with $\tau = 0.63 \pm 0.27$ and the second at $E=0.90 \pm 0.03$ keV with $\tau = 0.5 \pm 0.2$. Leighly et al. (1997b) also find evidence for one or more absorption features near 1 keV. The addition of a Gaussian emission line in the range 0.6–3 keV, instead of an absorption feature, does not provide any improvement in the fit.

NGC 4051

Previous investigations of the X-ray spectrum of NGC 4051 have suggested the existence of a warm absorber. There is no evidence for additional spectral features in the first observation (taken during the PV phase of the mission) but the second (AO2) observation, which has much better signal/noise ratio, does show significant features in the residuals between 0.7 and 0.9 keV. In this case we have modelled this apparent warm absorber with 2 absorption edges, for the first edge $E = 0.73 \pm 0.02$ keV and $\tau = 0.33 \pm 0.05$, for the second edge $E=0.93 \pm 0.03$ keV and $\tau = 0.19 \pm 0.04$. The resulting fit statistic is $\chi^2/\nu = 2010/1842$, an improvement of $\Delta\chi^2 = 77$ over the model without absorption. The results suggest a normal warm absorber in NGC 4051, with the edges probably originating from OVII and OVIII. Our results are broadly consistent with those of Guainazzi et al. (1996), who consider the fitting of this observation in much greater detail.

PG 1244+026

Emission and absorption components give comparable fits in PG 1244+026. The addition of a broad Gaussian absorption line significantly improves the fit ($\chi^2/\nu = 601/532$), as per Table 4. A single edge at an energy of $E=1.18 \pm 0.03$ keV, gives a better fit ($\chi^2/\nu = 591/533$). Adding another edge further improves the fit; with two edges (at $E=1.16 \pm 0.04$ keV and $E=0.63^{+0.04}_{-0.45}$ keV) the fit obtained is $\chi^2/\nu = 583/531$.

A broad Gaussian emission line at an energy of $E=0.97 \pm 0.04$ keV also significantly improves the fit ($\chi^2/\nu = 589/532$), with an equivalent width of $EW=36 \pm 11$ eV. A slightly better fit ($\chi^2/\nu = 586/533$) is obtained with the MEKAL model, with a plasma temperature of $kT=1.0 \pm 0.1$ keV. Fiore et al. (1998) also find evidence for either an absorption feature at ~ 1.2 keV or an emission feature at 0.9 keV.

IRAS 13224-3809

Absorption components give a slightly better fit than emission components. The addition of a single absorption edge to the model improves the fit significantly ($\chi^2/\nu = 478/424$). The best fit edge energy is $E=1.11 \pm 0.04$ keV. A second edge improves the fit further ($\chi^2/\nu = 467/422$), with edge energies at $E=1.00 \pm 0.04$ and 1.18 ± 0.03 keV and optical depths of $\tau = 0.73$ and 1.15 respectively. This fit also alters the continuum parameters slightly: $\Gamma = 1.84 \pm 0.07$ and $kT=163 \pm 9$ eV. A broad Gaussian absorption line gives a slightly better fit ($\chi^2/\nu = 459/423$), with parameters as in Table 4.

A broad Gaussian emission line at 0.74 ± 0.05 keV gives a slightly worse fit ($\chi^2/\nu = 470/423$), as does the MEKAL model ($\chi^2/\nu = 480/424$) with a plasma temperature of $kT=0.63 \pm 0.05$ keV. These results are broadly consistent with those of Leighly et al. (1997b).

PG 1404+226

Significant evidence is found for an absorption feature in PG 1404+226. The addition of a single edge to the best-fitting continuum model (PL+BB) yields $\chi^2/\nu = 172/165$, an improvement of $\Delta\chi^2 = 29$, with an edge energy of $E=1.07 \pm 0.03$ keV and optical depth $\tau = 0.84 \pm 0.28$, consistent with the results of Leighly et al. (1997b). A slight improvement ($\Delta\chi^2 = 8.1$) is also achieved by adding a second edge, although the edge energy of $E=2.4 \pm 0.3$ keV seems rather high. The 1 keV feature can also be modelled with a broad Gaussian absorption line, giving $\chi^2/\nu = 170/164$ with fit parameters as in Table 4.

An emission model (Gaussian line) is unacceptable as the broad emission feature essentially models the continuum soft excess and gives an unacceptably large equivalent width.

IRAS 17020+454

The residuals from a simple power law plus Galactic absorption fit show clear signs of absorption in IRAS 17020+454 (see Figure 2). The addition of an edge at an energy of $E=0.71 \pm 0.02$ keV with a depth $\tau = 0.91 \pm 0.22$, improves the fit significantly ($\chi^2/\nu = 979/971$). A second edge at $E=1.15 \pm 0.04$ keV with a depth $\tau = 0.20 \pm 0.08$ further improves the fit ($\chi^2/\nu = 965/969$). A broad Gaussian absorption line gives a comparable fit as detailed in Table 4.

A narrow Gaussian emission line at an energy of $E=1.06 \pm 0.02$ with an equivalent width of $EW=23^{+5}_{-7}$ eV gives a worse fit than an absorption line ($\chi^2/\nu = 1006/971$). However, the inclusion of an edge at 0.72 ± 0.02 keV, as well as the emission line, does lead to a net improvement in the fit ($\chi^2/\nu = 962/969$).

In agreement with Leighly et al. (1997a) we identify the 0.7 keV feature with an absorption edge from OVII. Komossa & Bade (1998) present a *ROSAT* spectrum of IRAS 17020+454 and also find evidence for a warm absorber, albeit a dusty one.

IRAS 20181-224

There may be an emission or absorption feature in the spectrum of IRAS 20181-224, but the improvement in the fit upon adding either is rather small. A broad absorption line gives a slight improvement in the fit, as noted in Table 4, but adding one or two edges in the range 0.6–3 keV gives a significantly a worse fit.

A narrow Gaussian emission line at 1.11 ± 0.05 keV also slightly improves the fit ($\chi^2/\nu = 438/387$). The MEKAL model gives a similar result with a plasma temperature of $kT=1.7^{+0.6}_{-0.3}$ keV.

Ark 564

Comparable fits are obtained with either a broad emission feature at ~ 1 keV or two absorption components. A single absorption edge at $E=1.23 \pm 0.02$ keV gives $\chi^2/\nu = 1862/1565$ whereas two edges improves the fit to $\chi^2/\nu = 1819/1563$ (the edge energies being $E=1.14 \pm 0.03$ keV and 1.37 ± 0.04 keV with $\tau = 0.18 \pm 0.04$ and 0.15 ± 0.03 , respectively). This is consistent with the Brandt et al. (1994) modelling of the *ROSAT* spectrum of Ark 564 which employed a deep absorption edge at 1.15 keV. The broad Gaussian absorption line model detailed in Table 4 is clearly not the best representation of the data ($\chi^2/\nu = 1854/1564$).

A broad emission line provides a slight improvement over two edges ($\chi^2/\nu = 1815/1564$) with $E=0.99 \pm 0.01$ keV, $\sigma = 0.10 \pm 0.03$ keV and $EW=39^{+8}_{-4}$ eV. The MEKAL model gives a worse fit ($\chi^2/\nu = 1830/1565$), with a plasma temperature of $kT=1.10^{+0.10}_{-0.05}$ keV.

The SIS and GIS detectors systematically diverge below 0.9 keV. There are also signs that the two SIS detectors are diverging at ~ 0.6 keV with SIS-1 seeming to underestimate the flux compared with SIS-0. These problems make it difficult to establish the nature of the soft X-ray spectral features in Ark 564.

This paper has been produced using the Royal Astronomical Society/Blackwell Science L^AT_EX style file.